Quaternary Science Reviews 29 (2010) 43–55

Contents lists available at ScienceDirect

Quaternary Science Reviews

journal homepage: www.elsevier.com/locate/quascirev

High-latitude climate sensitivity to ice-sheet forcing over the last 120 kyr

Joy S. Singarayer [a,b,*], Paul J. Valdes [a]

[a] Bristol Research Initiative for the Dynamic Global Environment (BRIDGE), School of Geographical Sciences, University of Bristol, University Road, Bristol, BS8 1SS, UK
[b] Bristol Glaciology Centre at the School of Geographical Sciences, University of Bristol, UK

ARTICLE INFO

Article history:
Received 15 January 2009
Received in revised form
19 October 2009
Accepted 20 October 2009

ABSTRACT

Interpretation of ice-core records is currently limited by paucity of modelling at adequate temporal and spatial resolutions. Several key questions relate to mechanisms of polar amplification and inter-hemispheric coupling on glacial/interglacial timescales. Here, we present the first results from a large set of global ocean–atmosphere climate model 'snap-shot' simulations covering the last 120 000 years using the Hadley Centre climate model (HadCM3) at up to 1 kyr temporal resolution. Two sets of simulations were performed in order to examine the roles of orbit and greenhouse gases versus ice-sheet forcing of orbital-scale climate change. A series of idealised Heinrich events were also simulated, but no changes to aerosols or vegetation were prescribed. This paper focuses on high latitudes and inter-hemispheric linkages. The simulations reproduce polar temperature trends well compared to ice-core reconstructions, although the magnitude is underestimated. Polar amplification varies with obliquity, but this variability is dampened by including variations in land ice coverage, while the overall amplification factor increases. The relatively constant amplification of Antarctic temperatures (with ice-sheet forcing included) suggests it is possible to use Antarctic temperature reconstructions to estimate global changes (which are roughly half the magnitude). Atlantic Ocean overturning circulation varies considerably only with the introduction of Northern Hemisphere ice sheets, but only weakens in the North Atlantic in the deep glacial, when ocean–sea-ice feedbacks result in the movement of the region of deep convection to lower latitudes and with the introduction of freshwater to the surface North Atlantic in order to simulate Heinrich events.

1. Introduction

Polar regions have in recent decades experienced temperature increases that are several times larger than the global average (Trenberth et al., 2007). Future climate change simulations demonstrate a range of polar amplification of global warming between 1.5 and 4.5 (Holland and Bitz, 2003). This amplification is a result of several factors including ice-albedo feedback, greater fractional changes in heating rather than evaporation at high latitudes, as well as impacts on ocean-to-atmosphere heat transfer from the changing sea-ice cover (ACIA, 2004). The Arctic and Antarctic Peninsula are consequently sensitive indicators of global change, and particularly vulnerable to such changes.

Past variations in polar temperature can be reconstructed from the water stable-isotope composition of ice in deep ice cores from the Arctic and Antarctic, scaled by borehole temperatures and gas fractionation to account for changes in seasonality (e.g. Masson-Delmotte et al. 2006a; Jouzel et al., 2007; Kawamura et al., 2007). Deep ice cores are unique in providing high temporal resolution data, which span several glacial cycles in the case of the EPICA (European Project for Ice Coring in Antarctica) and Vostok cores (Petit et al., 1999; EPICA community members, 2004). Recent temperature reconstructions from ice-core proxy data suggest that during the Last Glacial Maximum (LGM) temperatures at the EPICA dome C core site were 9 °C cooler than present day (Jouzel et al., 2007) and Greenland was 19–22 °C colder than present day (Masson-Delmotte et al., 2006a). During the mid-Holocene (6 kyr BP; MH) temperatures estimated from stable isotopes were up to 0.8 and 0.5–0.9 °C warmer than present over east Antarctica and central Greenland respectively (Masson et al., 2000, Masson-Delmotte et al., 2005). At the start of the last interglacial (130 ± 1 kyr BP; LIG) polar temperatures were much warmer than at present, 3–5 °C in central Greenland and roughly 4 °C at the EPICA site.

The question of how these orbital-scale high latitude temperature changes amplify global change, and what teleconnections and feedbacks are operating, can be investigated using climate models. The

* Corresponding author at: Bristol Research Initiative for the Dynamic Global Environment (BRIDGE), School of Geographical Sciences, University of Bristol, University Road, Bristol, BS8 1SS, UK. Tel.: +44 0 117 928 9068; fax: +44 0 117 928 7878.
E-mail address: joy.singarayer@bris.ac.uk (J.S. Singarayer).

0277-3791/$ – see front matter © 2009 Elsevier Ltd. All rights reserved.
doi:10.1016/j.quascirev.2009.10.011

Paleoclimate Model Intercomparison Project (PMIP1 and PMIP2; Braconnot et al., 2007a,b) simulations have been used to quantify polar amplification at the LGM, MH and pre-industrial (PI). For example, fully coupled ocean–atmosphere model LGM simulations from the second phase of the project (PMIP2) suggest an average polar amplification factor for Greenland of 2.7 (Masson-Delmotte et al., 2006b), due to changes in topography, albedo feedbacks and atmosphere/ocean circulation changes. Antarctic amplification from the same LGM model simulations was 2.1 (with no correction for elevation changes). A feature of all PMIP2 models is the underestimation of Greenland temperature change at the LGM, while some models do manage to capture the magnitude of Antarctic cooling. Central Greenland simulated LGM to PI temperature change was 6.2–14.5 °C, which is roughly half that obtained from stable isotopes; possibly a result of neglecting aerosol loading and vegetation changes in the model, which probably have greater impact over Greenland than Antarctica (Masson-Delmotte et al., 2006a).

Both Greenland and Antarctica temperature anomalies from the PMIP2 range of models were linearly related to the modelled global change. However, only a few scenarios have been extensively compared: the LGM and MH, as well as $2 \times CO_2$ and $4 \times CO_2$ scenarios (Masson-Delmotte et al., 2006b). The polar amplification factor was smaller for $2 \times CO_2$ and $4 \times CO_2$ scenarios than for the LGM. It has been suggested that the Antarctic in particular can be used to estimate global temperature changes over glacial–interglacial (G-IG) timescales, partly because it will be less sensitive to local changes in land surface cover, and the polar amplification makes it a sensitive indicator (e.g. Genthon et al., 1987; Masson-Delmotte et al., 2006b; Hargreaves et al., 2007). One interpretation of the PMIP2 results is that Antarctic temperature changes in ice cores may be used to represent global changes if divided by roughly a factor of two (Masson-Delmotte et al., 2006b). Antarctic climate change may also be useful to constrain global climate sensitivity (Hargreaves et al., 2007). Following PMIP2 and other studies, it would be useful to investigate the variability of polar amplification throughout the last glacial cycle.

The majority of modelling studies with general circulation models (GCMs) have focussed on key time periods in the last glacial cycle, such as the LGM and MH. Previous attempts at modelling the evolution of climate through the last glacial–interglacial cycle have used energy balance models (EBM) or Earth system models of intermediate complexity (EMIC) (e.g. Short and Mengel, 1986; Gallee et al., 1992; Tarasov and Peltier, 1999; Berger et al., 1998), or have used GCMs in which the boundary condition forcing is accelerated by up to a factor of 100 to cope with the large computational effort, although the internal timescales and physics of the model are unchanged (i.e. Jackson and Broccoli, 2003; Kutzbach et al., 2008; Lorenz and Lohmann, 2004). In most GCM-based simulations, the studies have so far only focussed on orbital forcing, using either a simple slab ocean model (Jackson and Broccoli, 2003) or a low resolution GCM (Kutzbach et al., 2008). Such models have demonstrated, for example, the importance of both orbital forcing and decline in atmospheric CO_2 for Northern Hemisphere ice volume (e.g. Berger et al., 1998), and the importance of sea-ice feedbacks in mid to high latitude response to orbital forcing to enable glaciation (Jackson and Broccoli, 2003). One recent study (Liu et al., 2009) used a GCM to model the evolution of the deglaciation from 21 kyr to 14 kyr, which highlighted the importance of changes in the Atlantic overturning and CO_2 to achieve the abrupt warming at the Bølling–Allerød transition.

In this study we present the first results from a large number of simulations with a fully coupled GCM that cover the last glacial cycle. We performed snapshot simulations at up to 1 kyr intervals over the time period 120 kyr BP to present. Two experiments were performed: in one experiment the orbital configuration and atmospheric greenhouse gas concentrations were varied, and in the other experiment variations in ice sheets were prescribed in addition. Primarily, climate changes on orbital timescales are examined, as the simulations are not fully transient. The only millennial-scale variation to be investigated is the impact of Heinrich events, which are modelled in a series of idealised freshwater hosing experiments. Here, in particular, we use these sensitivity experiments to address the question of the variability of polar amplification and mechanisms producing asymmetry in climate change in the Northern and Southern Hemispheres over the last 120 kyr BP.

2. Methods

2.1. General model description

We performed multiple "snapshot" simulations with the Hadley Centre climate model, HadCM3 (Gordon et al., 2000; Pope et al., 2000). HadCM3 is a state-of-the-art GCM that was heavily used in both the third and fourth assessment reports of the Intergovernmental Panel on Climate Change (IPCC, 2001, 2007). The GCM consists of a linked atmospheric model, ocean model and sea ice model. The resolution of the atmospheric model is 2.5° in latitude by 3.75° in longitude by 19 unequally spaced levels in the vertical. The spatial resolution over the ocean in HadCM3 is 1.25° by 1.25° by 20 unequally spaced layers in the ocean extending to a depth of 5200 m. The model contains a typical range of parameterisations in the atmosphere and ocean, including a detailed radiation scheme that can represent the effects of minor trace gases (Edwards and Slingo, 1996). The land surface scheme includes the representation of the freezing and melting of soil moisture, and terrestrial evaporation includes the dependence of stomatal resistance on temperature, vapour pressure and CO_2 concentration (Cox et al., 1999). In this version of the model, interactive vegetation is not included. The ocean model uses the Gent–McWilliams mixing scheme (Gent and McWilliams, 1990). The sea ice model uses a simple thermodynamic scheme and contains parameterisations of ice drift and leads (Cattle and Crossley, 1995). We extensively benchmarked our version of the model to ensure that it statistically gave the same control climate as previously published.

2.2. Boundary conditions

A complete Earth system model would be able to attempt to simulate the last glacial–interglacial cycle using orbital forcing only. However, the HadCM3 GCM does not include interactive ice, carbon cycle, or methane. Hence we must force the model with prescribed changes in orbit, greenhouse gases and ice-sheet evolution. The former two are relatively well constrained. Orbital parameters are taken from Berger and Loutre (1991) and were straightforward to include within the GCM. Similarly atmospheric concentrations of CO_2 were taken from Vostok (Petit et al., 1999; Loulergue et al., 2008) and CH_4, and N_2O were taken from EPICA (Spahni et al., 2005). All ice-core data were on the same EDC3 timescale (Fig. 1; Parrenin et al., 2007).

Ice-sheet extent and elevation, and associated changes in sea level and isostatic adjustment, are more poorly constrained, particularly for the period before the Last Glacial Maximum (21 kyr BP). For GCM modelling, we need to know the evolution of all of the major ice sheets and there are relatively few studies which have attempted to reconstruct together all of the major ice sheets, namely the North American, Greenland, Fennoscandian, and Antarctic ice sheets. We chose to develop our ice-sheet reconstructions using the ICE5G model of Peltier (2004). This was used by the PMIP2 project as a boundary condition for the LGM simulations. The dataset also includes a detailed evolution of the ice thickness, extent, and

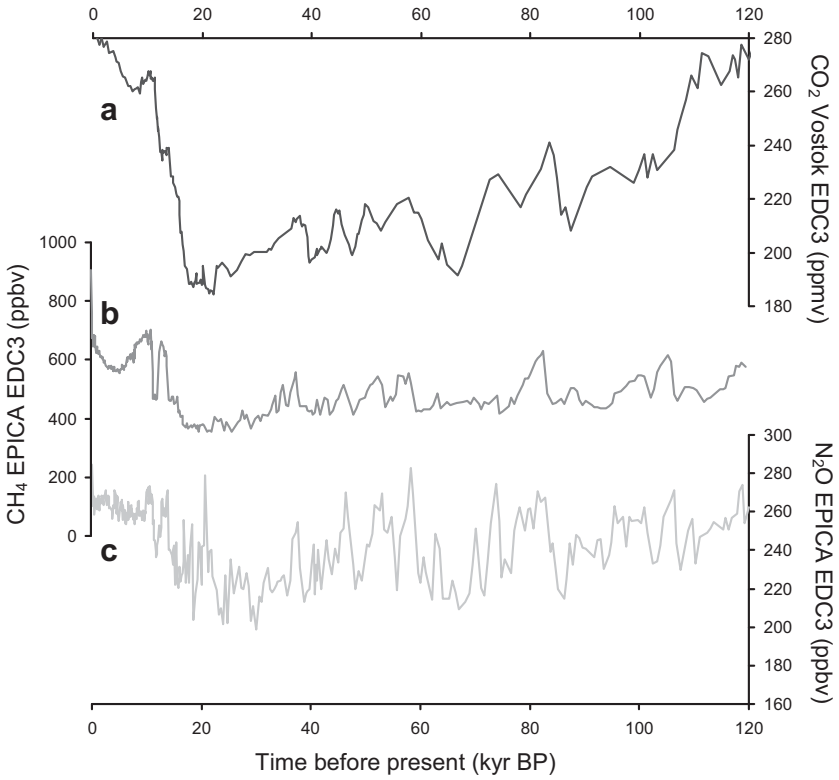

Fig. 1. Greenhouse gas atmospheric concentrations used as boundary conditions for the simulations (a) CO_2 from Vostok ice core (Petit et al., 1999); (b) CH_4; and (c) N_2O from EPICA ice cores (Spahni et al., 2005; Loulergue et al., 2008), all transferred to the EDC3 chronology.

continental isostatic rebound for the whole period from the LGM to the modern at 500 year intervals. Using standard linear interpolation techniques, this dataset can be used to calculate, at the GCM scale, the total continental elevation (including the direct thickness of the ice sheets plus the effects of isostatic adjustment), bathymetry (including isostatic changes), ice-area extent, and land sea mask for each time interval. To ensure consistency with existing pre-industrial boundary conditions, we used an anomaly-based method to calculate our palaeogeographic boundary conditions. In this method, anomalies of a particular time-slice palaeogeography minus pre-industrial ICE-5G data are then added to our model pre-industrial geographical boundary conditions.

Before 21 kyr BP it is more difficult to reconstruct the geographical extent and heights of the major ice sheets. We based our reconstructions on the work of Peltier and Fairbanks (2006), which included a calculation of the pre- and post-glacial ice. This work used the Martinsen et al. (1987) SPECMAP record of $\delta^{18}O$ history to constrain the evolution of the volume of land ice from the last interglacial up to the LGM. It assumed that during glaciation the area of the continents covered by ice remains similar to the LGM coverage and that ice thickness simply rises synchronously with $\delta^{18}O$. Thus our choice of reconstruction will have a tendency to overestimate ice extent, but has a total ice volume consistent with observations (Fig. 2). In addition, Peltier and Fairbanks (2006) suggested that the maximum ice volume occurs at about 26 kyr BP. We complemented the ice-sheet thickness data with regression analysis on the ICE5G dataset to produce the orographic height and bathymetry for each pre-LGM time period.

The ICE5G dataset is known to have some weaknesses. In particular, the reconstructed ice sheets are constrained by relative sea-level datasets and estimates of ice-sheet extent, but are generally not glaciologically constrained (except for Greenland; see Tarasov and Peltier, 2002). This means that the reconstructed ice sheets rarely have a parabolic edge consistent with most ice-sheet modelling, but instead have a relatively flat profile near the ice margin. Future work will investigate the sensitivity of our results to different methodologies for calculating ice-sheet extent and height.

2.3. Experimental set-up

We performed two sets of "snapshot" simulations each consisting of 62 model runs covering the whole of the last 120 000 years, at a frequency ranging from every 4000 years at the start of the period (between 120 kyr BP and 80 kyr BP), to every 2000 years from 80 kyr BP to 22 kyr BP and to every 1000 years from 22 kyr BP to the pre-industrial. One set of simulations includes forcing from changes in greenhouse gases and orbital parameters

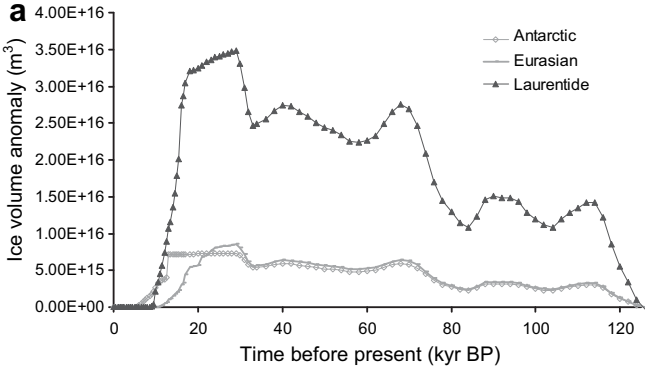

Fig. 2. Volume anomaly from pre-industrial of the major ice sheets used as boundary conditions in the model simulations: Eurasian (line symbols), Antarctic (open circle symbols) and Laurentide/North American (filled triangle symbols) ice sheets.

(this set will hereafter be called ORB-GHG). These forcings are relatively well known. We also have additional simulations for the period 120–140 kyr BP for the ORB-GHG experiment. The second set of simulations also includes the changes in ice-sheet height and area, sea level, and bathymetric changes as described above (this set will hereafter be called ALL).

For each simulation, the boundary condition forcings (orbit, greenhouse gases, and ice sheets) were specified, and in all simulations the initial conditions were the same, based on a spun-up pre-industrial simulation. When land sea mask and bathymetry changes were included, simple bi-linear interpolation was used to fill in new ocean grid points and grid points that changed from ocean to land were set to undefined. There was no attempt to conserve global heat or salinity between each simulation although the model does conserve these during each run.

After initialising the model with pre-industrial conditions, each simulation was run for 500 years. At this stage, the trends in surface temperature were small (in all cases less than 0.002 °C per year (0.2 °C per century) and in most cases less than 0.0005 °C per year (0.05 °C per century); see Fig. 3a inset). Although not in perfect equilibrium (most GCMs are never truly in equilibrium), we judged that we were close enough for the models to be representative of the time period (Fig. 3a,b). The 500 year length of integration was typical of many models used within the PMIP2 project. The approach of using the same initial conditions for all simulations is acknowledged as being a non-ideal methodology, but the compromise was necessary to allow us to run the simulations simultaneously, meaning it took only a few months to complete the total set. The results presented here are climatologies of the last 30 years of each simulation.

The strength of our modelling procedure is that we used an IPCC-standard model and that we had good spatial resolution in our model results. However, it is important to appreciate some of the limitations and caveats about this procedure. The version of HadCM3 that we used does not include interactive vegetation so all the simulations use the same pre-industrial vegetation boundary condition. We will investigate the importance of vegetation feedback in a subsequent study. Similarly we do not change aerosol loading so the model does not account for changes in dust during the cycle. We have not attempted to represent millennial-scale variability such as Dansgaard–Oschger events, as they occur on a finer temporal resolution than our snapshot simulations and the mechanisms are poorly understood in any case. However, additional simulations were run to capture climate change due to Heinrich event iceberg discharges resulting in shutdown of the thermohaline circulation. There are currently thought to have been six occurrences of Heinrich events during the last glacial cycle. To simulate the input of freshwater following major iceberg rafting of Heinrich events, 1 Sv of freshwater was continuously added to the surface layer of the ocean model in the Atlantic between 50°N and 70°N latitude for 200 years as a continuation from the initial ALL equilibrium simulations for time slices, 17, 24, 32, 38, 46, and 60 kyr BP. These represent roughly the timings of ice-rafted debris found in ocean sediment cores (Hemming, 2004). However, the magnitude and duration of freshwater inputs are poorly known, so these simulations should be viewed as idealised. The forcing is typical of many previous studies (e.g. Hewitt et al., 2006).

Notwithstanding the additional Heinrich event simulations, the modelling approach we have adopted assumes that the climate is in equilibrium at each time period, and that it is

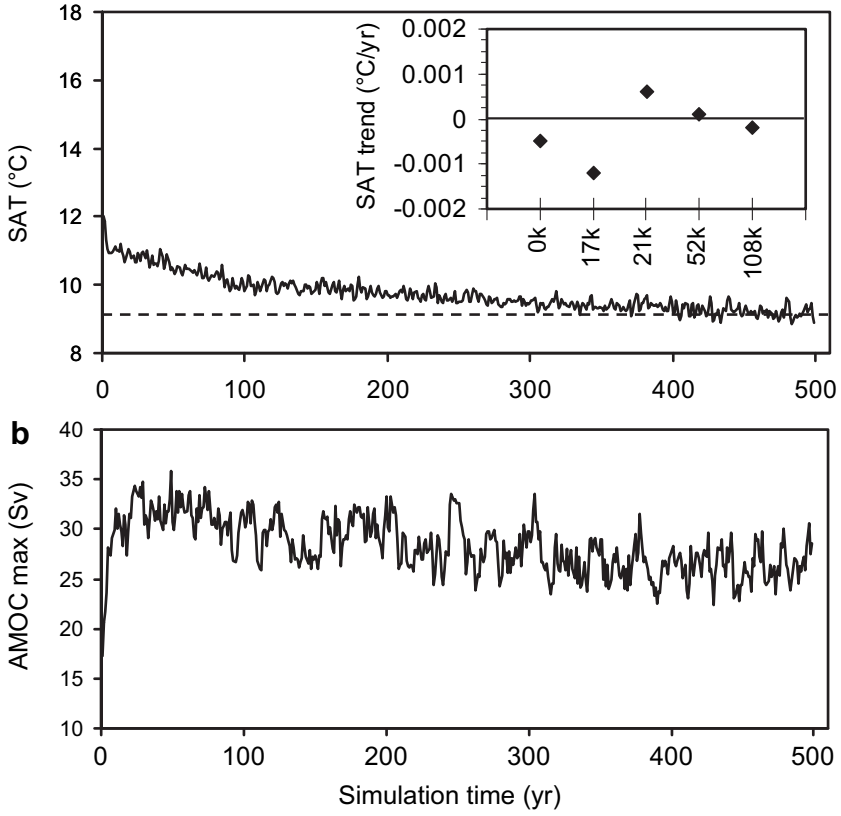

Fig. 3. Annual average time series results for the 500 year simulation with 34 kyr BP boundary conditions, starting from pre-industrial initial conditions. (a) Global mean surface air temperature (black line) and equilibrium temperature (9.3 °C). Inset shows the linear trend in SAT for five of the simulations in the ALL set. The trend was calculated over the last 100 years, and shown as degrees C per year; (b) Atlantic meridional overturning circulation maximum index.

insensitive to initial conditions. The assumption of equilibrium has some similarities to the assumptions behind accelerated forcing simulations, and has been partially justified by Lorenz and Lohmann (2004) and Lunt et al. (2006). Studies by Bigg et al. (1998) and Rahmstorf et al. (2005) have shown sensitivity of models to the initial condition of the ocean. However, such results have largely been confined to EMICs or ocean only models. It is relatively rare (one example is Stouffer and Manabe, 2003) to find multiple equilibria in full complexity GCMs. Previous freshwater hosing experiments with HadCM3 have displayed no evidence of multiple stable states (e.g. Vellinga and Wood, 2002), hence we assume that our simulations are a reasonable first approximation to the climate for each period and represent the first time that a relatively high resolution GCM has been used to investigate the entire glacial–interglacial cycle.

3. Results

3.1. Global and polar temperatures

Initial analyses of the modelled global annual mean temperature variations over the last glacial cycle are displayed in Fig. 4a. Shown as anomalies from pre-industrial, the G-IG temperature range is 4.25 °C in experiment ALL. This is similar in magnitude to other estimates from PMIP2 models (3.6–5.7 °C LGM to pre-industrial temperature difference; Braconnot et al., 2007a) and a previous study with HadCM3 for the LGM (3.8 °C in Hewitt et al., 2001), and to synthesised data from multiple proxies of between 4 and 7 °C (Jansen et al., 2007). The temperature anomalies in experiment ORB-GHG are just under half the magnitude of experiment ALL during the glacial (Fig. 4a), but are relatively smaller than ALL during glacial inception than at glacial maximum. The early presence of ice sheets, and resulting change in surface albedo, in the model has a relatively greater effect on temperatures at the onset of glaciation, whereas the large decrease in CO_2 is more important in setting LGM temperatures than early in the glacial cycle. Both experiments share the same general features in global temperature anomalies, such as temperature minima at 66 kyr BP and 21–25 kyr BP. This is partly due to the inclusion of variations in atmospheric CO_2 in both experiments, which co-varies approximately with ice-sheet volume.

In order to provide a better comparison to data-based reconstructions from deep ice cores, we plotted annual mean temperature anomalies over central Greenland (Fig. 4b) and east Antarctica (Fig. 4c). In the case of Greenland temperature anomalies, the ORB-GHG G-IG temperature range is only up to a factor of 0.3 of experiment ALL. The G-IG temperature range in experiment ALL is 13.5 °C, which is towards the higher end of the PMIP2 model range (Masson-Delmotte et al., 2006b). Unlike global temperatures, there are some differences between ORB-GHG and ALL in terms of their structure through time. For example, this is especially prominent in marine isotope stage (MIS) 2, starting 30 kyr BP, when the ALL experiment displays a large decrease in temperature of a further 3 °C that is absent in ORB-GHG. This is partly a result of increased elevation in central Greenland in the prescribed ice sheets, but also a result of changes in ocean overturning circulation and local climate that occur due to the presence of large ice sheets at this time (which provide roughly two-thirds of the extra cooling at this time). This will be discussed further in Section 3.3.

The G-IG temperature range at east Antarctica is smaller by comparison, at ~7.5 °C. The temperature trends of ORG-GHG and ALL follow each other more closely in Antarctica than Greenland and vary with obliquity. The differences in the shape of the time series for simulated Greenland and Antarctic annual mean temperatures is due to the influence of the large expanse of ice sheets in the Northern Hemisphere compared to limited change in the Southern Hemisphere. In their respective winter seasons (with zero insolation) temperatures in Antarctica respond to CO_2 concentrations, whereas Greenland follows Northern Hemisphere ice volume more closely.

At both Greenland and Antarctica the G-IG temperature anomalies are underestimated compared to recent stable-isotope ice-core temperature reconstructions by Masson-Delmotte et al. (2006a) and Jouzel et al. (2007), and borehole measurements (Dahl-Jensen et al., 1998). Simulated Antarctic G-IG temperature range in the ALL experiment is smaller than the data reconstructions by up to 1.5 °C, and Greenland by up to 10 °C. There is clearly less high frequency structure to our simulated temperatures than the ice-core reconstructions as there was no forcing introduced to simulate Dansgaard–Oschger events. The six freshwater hosing simulations performed to represent Heinrich events (Fig. 4b; large black symbols) appear to partially reconcile the model-data discrepancy over Greenland. The addition of 1 Sv freshwater into the North Atlantic results in a collapse of the overturning circulation, and decreases the annual mean temperatures over central Greenland between 6.5 °C and 9 °C for H1-6. However, there is still a warm bias, with H3–H6 being warmer than the proxy-based reconstruction by 3–4 °C. The simulated time series of temperature anomalies in Fig. 4b are in general similar to the temperatures of warm phases of millennial-scale oscillations in MIS2 and MIS3 rather than the longer cold phases. There is, however, proxy evidence that at the LGM Greenland temperatures were over 20 °C cooler while the AMOC was reduced but still active, which the simulations are unable to recreate. Both large freshwater discharges and background routing (Meissner and Clark, 2006) may play a role in reducing ocean overturning circulation and reducing temperature in the North Atlantic. In the Antarctic the bipolar seesaw mechanism results in elevated temperatures during Heinrich events, as observed in ice-core proxy records, although our simplified hosing approach does not achieve the magnitude of temperature changes reconstructed from the data.

Although the inclusion of some millennial variability improves the model–data agreement, there are further points for consideration. For example, the temperature decrease may actually be underestimated in the Greenland ice-core stable-isotope reconstruction, as any change in seasonality of precipitation/snowfall is important in terms of accumulation and annual averaging of the water isotope signature (Krinner and Werner, 2003). This may increase the difference between model and data reconstructions. The temperature reconstructions from GRIP (Masson-Delmotte et al., 2005) accounted for changes in precipitation seasonality and source/site temperature using isotopic information combined with model estimates, and found good agreement at the orbital and millennial scale with temperatures from LGM borehole measurements and gas thermometry.

For these HadCM3 experiments we estimated the impact of seasonal accumulation changes on the proxy record by precipitation weighting the monthly mean temperatures to obtain precipitation-weighted annual average SATs. We found significant changes in the modelled seasonal cycle of precipitation between Glacial and Interglacial (Fig. 5a), with markedly decreased contribution in winter to the annual average, as previous studies have found (e.g. Masson-Delmotte et al., 2005). The largest SAT changes also occur in the winter months (Fig. 5b). As a result, weighting modelled monthly temperatures by precipitation to obtain annual mean temperature changes underestimates the modelled G-IG range (Fig. 5c) because a greater proportion of precipitation falls in early summer when temperatures are warmer. The larger the temperature decrease the larger the effect becomes (Fig. 5d), although

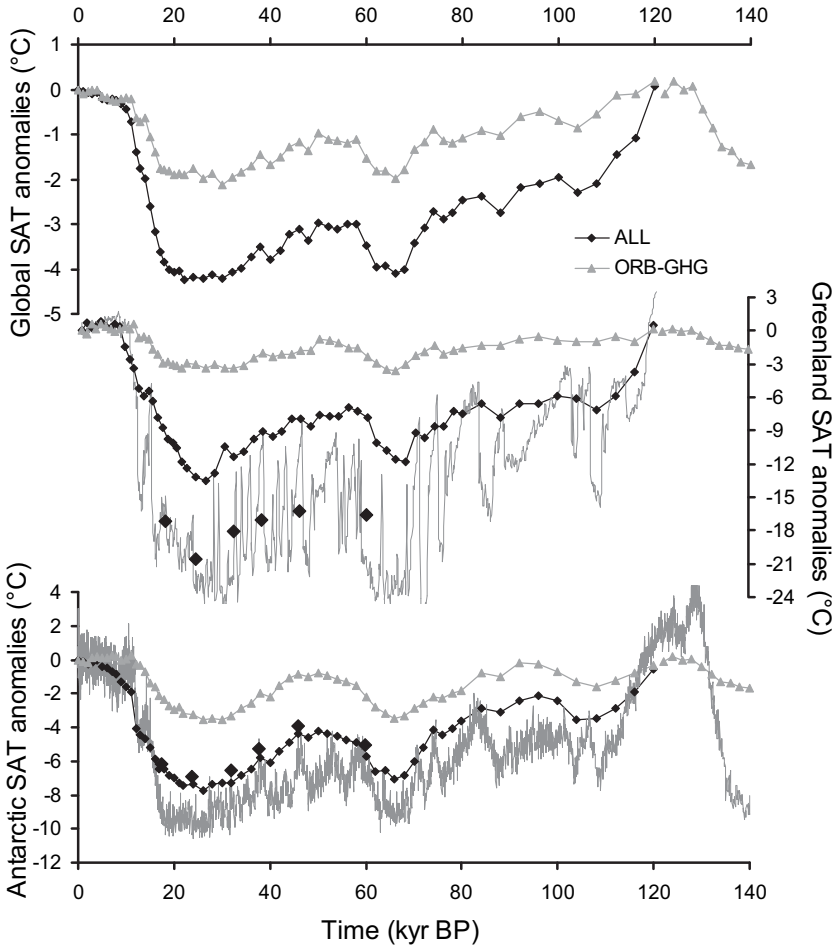

Fig. 4. Annual mean surface air temperature anomalies from pre-industrial for all time-slice simulations covering the last 140 kyr. Results for the ORB-GHG experiment are shown in grey triangles, and the ALL experiment results are black diamonds/lines for: (a) Global; (b) central Greenland (70–80°N, 60–20°W); and (c) east Antarctic (75–85°N, 100–160°W). Ice-core temperature reconstructions for Greenland (GRIP) and Antarctica (EPICA dome C) are shown as grey lines (Masson-Delmotte et al., 2005; Jouzel et al., 2007). Anomalies due to imposed 'Heinrich' freshwater hosing are given by the large black symbols.

interestingly the differences between annual mean temperature and precipitation-weighted temperature are much smaller than those determined in the ice-core reconstructions (Masson-Delmotte et al., 2005). This may be due to competing effects of source and site temperature on the isotopic signature, and would be possible to investigate in a further study through the inclusion of the water isotope component of the climate model. The same seasonality effect was more exaggerated for the Heinrich simulations (as demonstrated in Fig. 5d, dotted circle). In this case, precipitation weighting of SATs negated virtually all of the actual SAT decrease (Fig. 5c). It is possible that such changes in seasonal accumulation affect the expression of Heinrich event temperature changes over Greenland. Indeed, at times when ice-rafted debris related to Heinrich events is recorded there is often very little further decrease in temperature proxies in response.

Reconstruction of ice-sheet elevation and related temperature changes is one further consideration in model–data discrepancy. Masson-Delmotte et al. (2006a) suggested that although some models represent Antarctic temperature changes reasonably, the reason for this is partly due to the increased local elevation of the ICE-5G topography at the LGM (400 m; Peltier, 2004), which is not reconciled with elevation changes derived from ice-core air content data (Martinerie et al., 1994). In the PMIP2 models this was estimated to constitute 3.5–4 °C cooling. Observations of modern vertical lapse rate at the poles are between 6 and 15 °C per 1000 m (Krinner and Genthon, 1999) depending on season and location. The impact of elevation increase in the model will be a large proportion of the difference between our ORB-GHG and ALL experiments. Even accounting for possible errors in elevation change, the Antarctic temperature anomalies are closer to the data reconstructions than the results for Greenland. Two other factors missing from our modelling approach that are likely to impact Greenland more than Antarctica are changes in vegetation and aerosols. Crucifix and Hewitt (2005), for example, demonstrated that changes in vegetation enhance cooling of Northern Hemisphere at LGM.

The two interglacial periods included in our study, the Holocene and Eemian, display warmer polar temperatures than PI, in agreement with data. Greenland in the MH is up to 0.8 °C warmer in the model, and since there is little difference in ice-sheet volume, ORB-GHG and ALL experiments display similar results. In the Eemian (only simulated under the ORB-GHG set-up), Greenland temperatures are 1 °C warmer (at 124 kyr BP) and Antarctic temperatures warmer by 0.6 °C (maximum at 128 kyr BP). The different timing of maximum interglacial warmth in the Eemian at the poles is due to the larger influence of obliquity over high-latitude Antarctica, which is at a maximum at ~130 kyr BP, whereas Greenland temperatures are influenced more by North Atlantic conditions, which are warmer at 124 kyr BP as the AMOC intensifies (this intensification was noted by McManus et al., 2002; and could

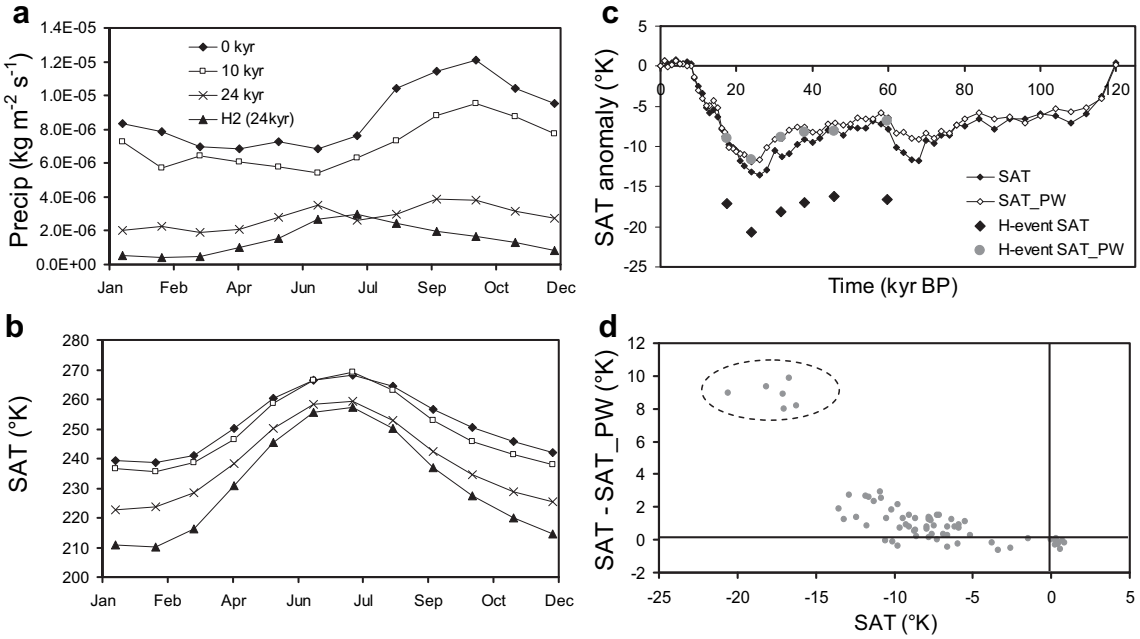

Fig. 5. (a) Seasonal cycle of precipitation over central Greenland (70–80°N, 60–20°W) for four time slices, including Heinrich event 2; (b) same as (a) but for surface air temperature; (c) the impact of precipitation weighting on Greenland SATs to approximate changes in seasonal accumulation; and (d) the impact of precipitation weighting of SATs (SAT_PW) compared against actual modelled SAT anomaly. The dotted grey ellipse encompasses the Heinrich event simulations as opposed to the main ALL simulation set.

be the cause of an increased moisture source for glacial inception post-124 kyr BP). Currently, without ice-core information as far back as the early Eemian for Greenland we cannot say whether the data agree with the model findings. However, it is clear that the magnitude of Eemian warmth at Antarctica is significantly underestimated. At 128 kyr BP there was a rapid warming up to 4–5 °C higher than pre-industrial. This coincides with a high sea-level stand of 4–6 m above present day (Overpeck et al., 2006). Ice-sheet and climate model simulations by Otto-Bliesner et al. (2006a) for this time period imply that a reduction in Greenland ice-sheet volume could have contributed 2.2–3.4 m of this. The use of modern Greenland and Antarctic ice-sheet distributions in our Eemian simulations, and the subsequent underestimate of Eemian warmth, suggests that in order to simulate the magnitude of the warming a retreat of ice sheets may be necessary. A recent modelling study by Holden et al. (submitted) covering several glacial cycles found that they could only reconcile modelled Antarctic temperatures with ice-core records if a significant loss from the West Antarctic Ice Sheet is prescribed. Holden et al. (submitted) found that precipitation weighting of Antarctic temperatures, to account for changes in seasonal accumulation having removed some of the West Antarctic ice sheet, provided additional apparent warming to further improve the model–data agreement. There may also be a component of ocean reorganisation causing the abrupt warming, similar to H1 during the last deglaciation.

3.2. Polar amplification

Polar amplification is defined as the ratio of temperature change in polar regions to the global average change. In reference to future climate change, this is usually defined as a response to a global forcing. However, in this study we use the term more loosely to investigate the response to orbital, greenhouse gas and ice-sheet forcing with the aim of examining how variable polar change is relative to global change in the model over the last glacial cycle (as Masson-Delmotte et al., 2006b, investigated for the LGM). Additionally, we want to assess whether ice-core data from either hemisphere can be used to estimate global temperature change over this time period. Time series of polar amplification factors relative to pre-industrial for Greenland and Antarctica for both ORG-GHG and ALL experiments are shown in Fig. 6. To avoid random anomalous values for those times when there is negligible global change (e.g. Holocene), only values where the global mean temperature change is over 0.5 °C have been included in the plot.

The inclusion of G-IG ice-sheet evolution results in a larger polar amplification factor over Greenland than Antarctica (Fig. 6a). Without this source of asymmetry, the ORB-GHG experiment produces equal amplification of global change at both poles (Fig. 6b). In the ORB-GHG experiment polar amplification varies throughout the glacial cycle from roughly 0.5 to 2 with a frequency that corresponds to obliquity forcing. When tilt is at a minimum polar amplification reaches a maximum, as a result of increased summer snow and sea-ice cover at high latitudes. At times of maximum tilt, the annual average polar SAT is a combination of warmer summer temperatures and slightly cooler winter temperatures. At lower latitudes there is a temperature decrease in all months compared to pre-industrial. The consequence of this is an annual mean polar change that is smaller than the global average, i.e. a polar amplification factor <1 is found when obliquity is high.

By comparison the polar amplification in the ALL experiment is less dominated by obliquity over the glacial cycle, especially over Greenland. As well as the Greenland amplification factor being greater than the Antarctic, there is also at times anti-correlation between the two hemispheres (e.g. 40–60 kyr, 90–100 kyr BP), and a larger Greenland amplification during much of OI stage 2 (20–30 kyr BP). This is due partly to the extensive Northern Hemisphere ice-sheet volume, which leads to an increase in sea-ice cover around Greenland (Fig. 8) and reduced Atlantic overturning circulation at high northern latitudes (see Section 3.3) during OI stage 2, further reducing temperatures over Greenland relative to the global mean.

It has been suggested that Antarctic temperatures and tropical ocean temperatures provide the best estimate of global G-IG climate change, and the best regions to constrain climate sensitivity

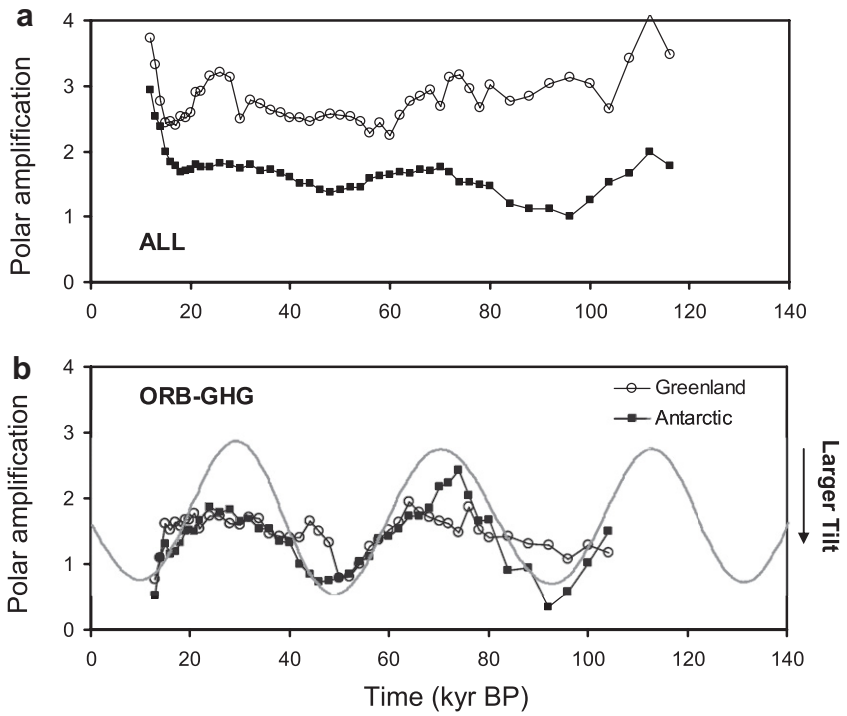

Fig. 6. Polar amplification of global temperature changes for all time slices covering 120 kyr at the central Greenland (open circles) and east Antarctic (filled squares) regions for the ALL (a) and ORB-GHG (b) experiments. The amplification factor is calculated as changes in temperature at the polar region divided by the global temperature change from pre-industrial. Grey line in (b) is the trend in obliquity, with higher values towards the bottom of the plot.

with palaeo-data (Masson-Delmotte et al., 2006b; Hargreaves et al., 2007). Antarctica is also less affected than other regions by atmospheric advection processes, and its isolation from other landmasses means it will not be readily affected by vegetation, dust and other feedbacks. Global temperature change has previously been estimated as half the Antarctic temperature change (Masson-Delmotte et al., 2006b). We find here that over much of the glacial cycle the Antarctic polar amplification factor in the ALL experiment remains relatively constant at just less than two (~1.6–1.8). This is slightly lower than suggested by the data, primarily because our Antarctic temperatures are underestimated by a couple of degrees. Given an extra ~2 °C cooling to Antarctic SATs, polar amplification would increase to be in better agreement with the magnitude estimated from the data. In our simplified representation of the last glacial cycle it would be reasonable to a first order approximation to estimate global temperature change from Antarctic temperatures. However, on sub-orbital timescales there will be some impact on polar amplification from ocean reorganisation. Greenland polar amplification is more variable and influenced by local changes in the North Atlantic region, even without considering the impact of dust/vegetation changes or millennial-scale events to allow any estimates of large-scale temperature change to be made. Additionally, modelling of Heinrich events described in the section below demonstrates that the bipolar seesaw warming of Antarctica reduces Antarctic polar amplification from 1.8 to 1.3 on average.

3.3. Thermohaline circulation and sea ice

Simulated polar temperatures demonstrate that the presence of large ice sheets in the Northern Hemisphere introduces significant asymmetry into the modelled climate system. In this section we discuss the impacts on large-scale ocean circulation which is one of the mechanisms that may transmit these to lower latitudes.

The pre-industrial Atlantic meridional overturning circulation (AMOC; Fig. 7a) in experiment ALL has a maximum value of 17.7 Sv at ~35° north, and at the depth of ~900 m. By comparison, the LGM NADW formation occurs at lower latitudes (Fig. 7b). The overall maximum NADW is stronger and slightly deeper at the LGM than pre-industrial, but at higher latitudes (40–70°N) the overturning is weaker and shallower. AABW is stronger at the LGM and extends further north. Proxy records from ocean sediment cores have been interpreted as suggesting a much weaker, shoaled NADW at the LGM (Curry and Oppo, 2005), or similar strength to present (McManus et al., 2004, suggest probably less than 30% difference), and there is a prevailing view that the bottom of the Atlantic was filled with dense southern-sourced AABW beyond 30°N. PMIP2 ocean–atmosphere models have shown a large range of responses to LGM boundary conditions, from a much weaker AMOC to negligible differences, to much stronger, deeper overturning than pre-industrial (Weber et al., 2007). HadCM3 simulations within the PMIP2 framework displayed little change between LGM and PI. Hewitt et al. (2001) found the same structure as we did in this study. The lack of shoaling of the NADW may relate to the fact that the PI NADW is already quite shallow (shallower than observations suggest; Hewitt et al., 2001; Otto-Bliesner et al., 2007), and even with PI boundary conditions the simulated AABW extends quite far north (30°N)

We find that there is a high degree of variation throughout the last glacial cycle of the maximum strength of North Atlantic Deep Water (NADW) and Antarctic Bottom Water (AABW), as shown in Fig. 7d for experiment ALL. A large proportion of this variation is due to the changing ice-sheet volume and sea level, since by comparison the ORB-GHG experiment shows much reduced variation in NADW and AABW (Fig. 7e). Both ORB-GHG and ALL experiments show that the response of the NADW in the model is to get stronger overall as the climate cools, i.e. the glacial circulation is stronger than pre-industrial. In the ORB-GHG experiment

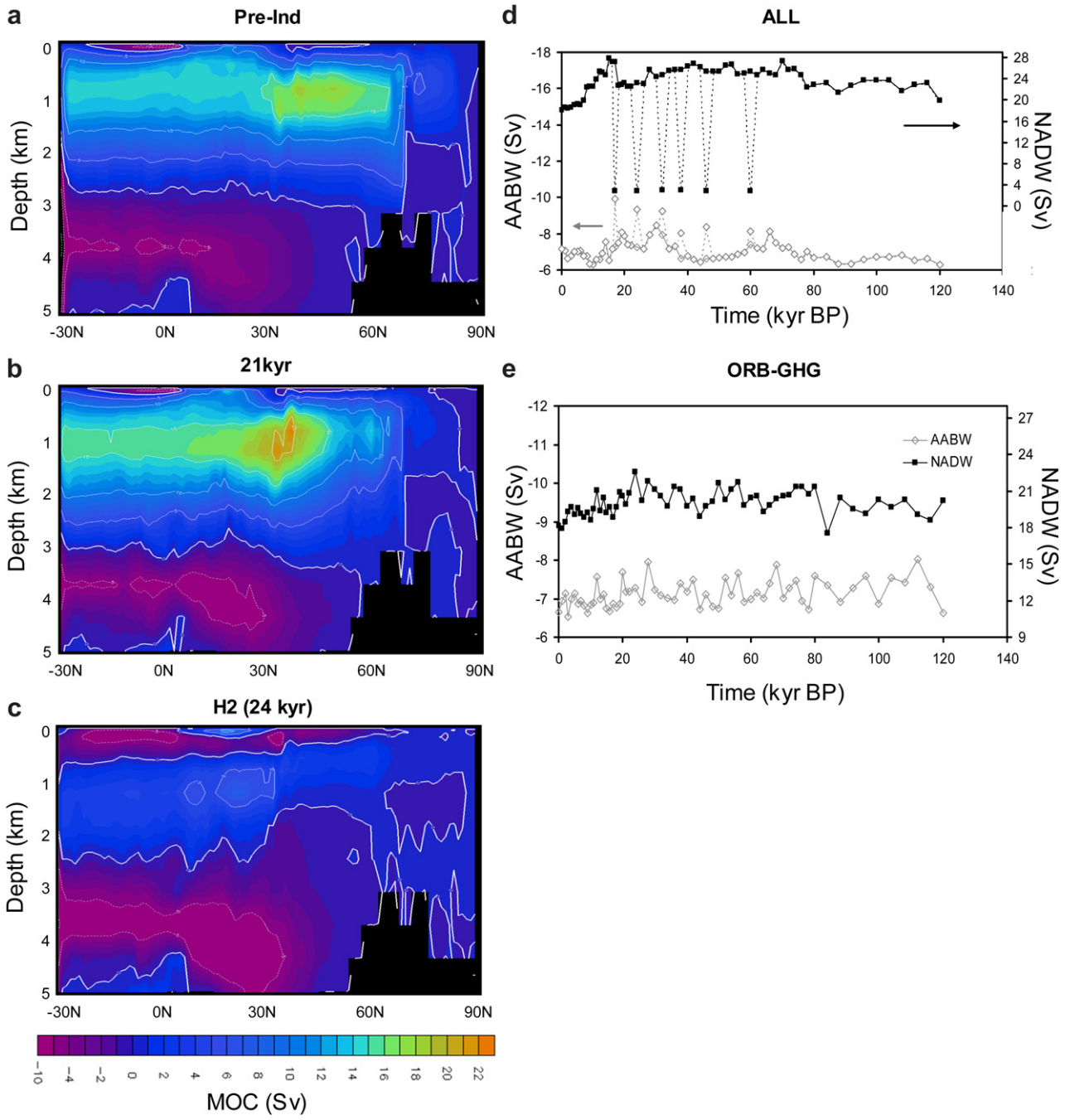

Fig. 7. Ocean overturning circulation results: Atlantic meridional overturning circulation with (a) pre-industrial boundary conditions, (b) LGM (21 kyr BP) conditions, and (c) Heinrich event 2 at 24 kyr conditions in experiment ALL. (d) Maximum North Atlantic overturning index (North Atlantic Deep Water; NADW) and maximum Antarctica Bottom Water (AABW) for all time slices covering the last 120 kyr in the ALL experiment. The dotted lines and symbols represent NADW/AABW following Heinrich event simulations. (e) Same as (d) for the ORB-GHG experiment.

there is no discernable cyclic behaviour on a sub-100 kyr time-scale, and a large proportion of the shorter time-scale variability may be due to the averaging process, which used the last 30 years for each simulation. In experiment ALL the AABW reaches maxima at 20–30 kyr BP and at around 60–70 kyr BP, concurrent with maximum ice volume in the Northern Hemisphere and minimum obliquity. At these two time periods the maximum NADW decreases, although still stronger than PI overturning. However, at any particular location there is a higher degree of variability than suggested by the maximum NADW for the whole of the North Atlantic. Time series of maximum NADW at 50°N (Fig. 9b) shows LGM values slightly weaker than PI than the absolute maximum (Fig. 9a). At this latitude the depth of deep convection is also shallower at the LGM than PI (Fig. 9d).

The evolution of each 500 year simulation elucidates the mechanisms important for AMOC variation between different time slices. Within a few years the AMOC becomes stronger in the glacial than the pre-industrial initial conditions (e.g. Fig. 3b). Fast cooling of the atmosphere at high latitudes initially leads to increased sea–air sensible and latent heat flux in the North Atlantic and results in colder, denser waters advecting into the regions of deep convection. Following this, the region of deep convection at northern high

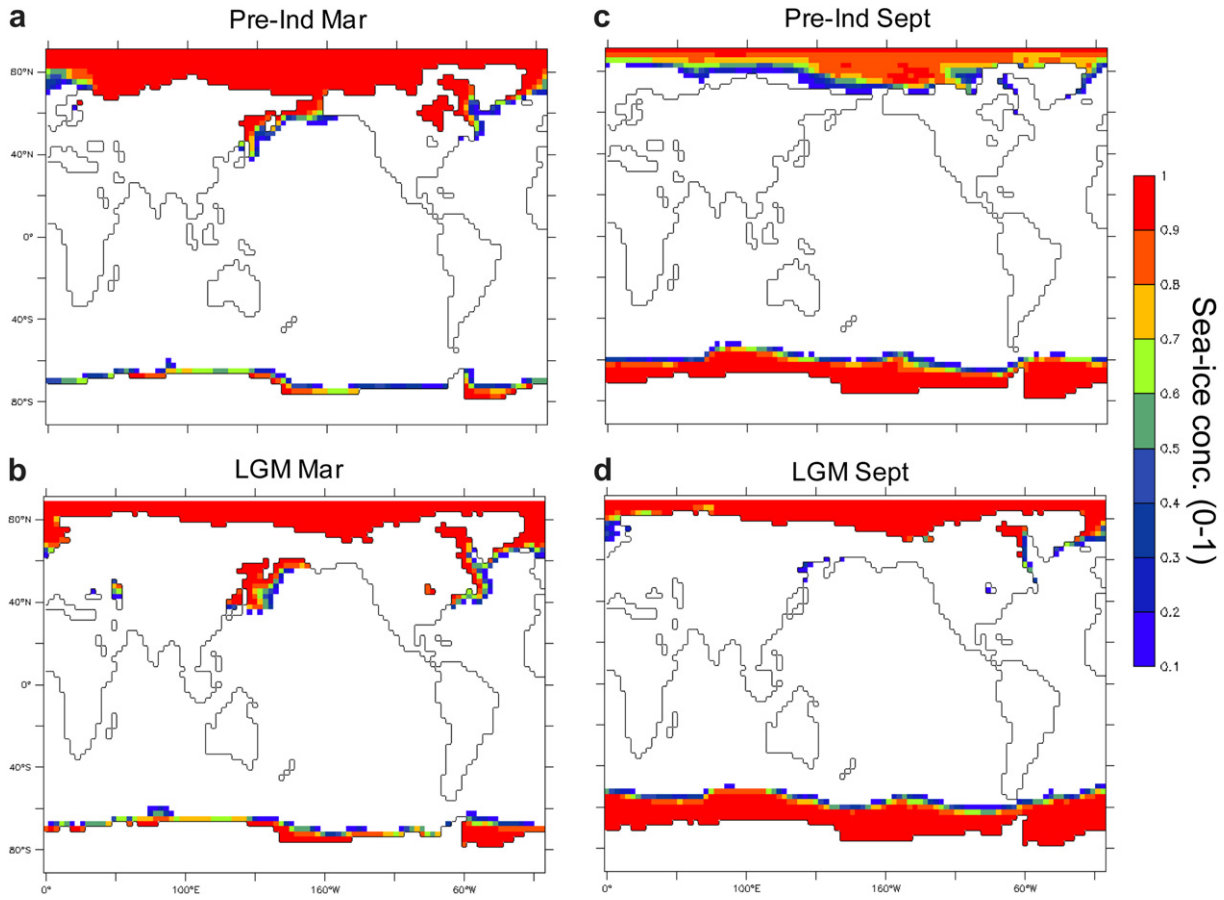

Fig. 8. Maps of maximum winter and summer sea-ice concentrations for the pre-industrial, (a) and (c), and LGM, (b) and (d). Sea-ice concentration is given a fraction of grid box area covered by ice.

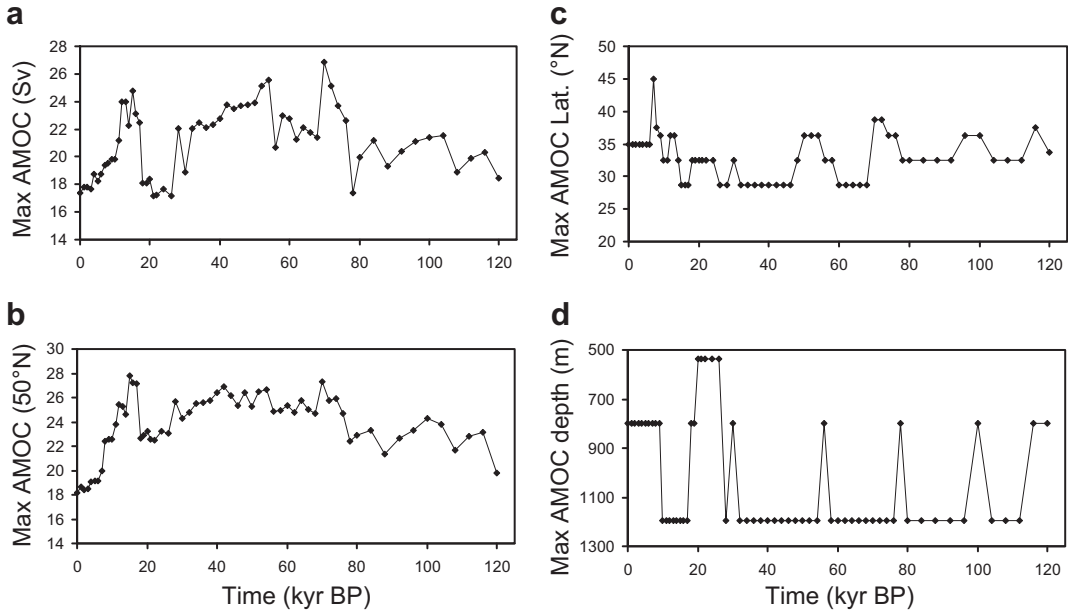

Fig. 9. Various characteristics of the Atlantic overturning circulation: (a) maximum overturning strength in the North Atlantic, (b) overturning strength at 50°N, (c) latitude of maximum overturning strength, and (d) depth of maximum overturning strength at 50°N.

latitudes in the ALL experiment moves further south as a delayed response of the ocean to the larger ice-sheet volume (also found by Hewitt et al. (2001) for the LGM). Lower regional temperatures result in increased sea-ice formation in the Greenland–Iceland–Norwegian (GIN) Seas, which prevents the release of ocean heat to the atmosphere (see Fig. 8 for a comparison of pre-industrial and LGM sea ice). Modelled sea-ice cover in the North Atlantic and Antarctic for the LGM compare well with estimates of ice extent from microfossil data (Sarnthein et al., 2003; Gersonde et al., 2005). At the LGM, the main region of deep convection moves to the Labrador Sea and sub-polar North Atlantic in a coupled process that takes several hundred years to reach equilibrium from initial conditions. Sea-ice concentrations in the Labrador Sea decrease in response to increasing winds caused by increased anticyclonic circulation over the Laurentide ice sheet. In general, overturning in the North Atlantic is stronger in the glacial because the colder atmosphere in the North Atlantic increases the ocean–atmosphere temperature gradient and increases ocean heat loss to the atmosphere in the region of deep convection. However, when temperatures in the GIN Seas become so cold that sea-ice formation prevents deep convection in that region (e.g. 20–30 kyr BP), the movement of the site of maximum mixed layer depth further south coincides with a decrease in overturning (although still stronger than PI) and an increase in AABW. This overall southward drift of the maximum AMOC from 120 kyr to 20–30 kyr BP is demonstrated in Fig. 9c.

The reorganisation of deep water formation in the North Atlantic as a result of the presence of glacial ice sheets results in large changes in climate locally and down to low latitudes. By looking at the changes in average climate throughout each 500 year simulation, we can estimate the oceanic influence, as climate changes related to deep ocean circulation will take longer to happen than changes solely relating to ice-sheet forcing of the overlying atmosphere. For 20–30 kyr BP simulations within the ALL experiment the movement of deep convection into the sub-polar North Atlantic results in temperatures over central Greenland cooling by up to 2 °C. The reduction in surface air temperature (SAT) extends down to mid-latitude North Atlantic storm track regions. In the 30–60 kyr BP simulations, where NADW is more vigorous and formation occurs in the GIN Seas, cooling of SATs across Western Europe is also mitigated to some extent.

The combination of these processes produces a complicated pattern of change in overturning circulation (Fig. 7d). The strength of NADW and AABW do not show a simple anti-correlated relationship in either ORB-GHG or ALL experiments, except during modelled Heinrich events. Neither the strength of AABW nor NADW is solely related to density of either water source or of the density contrast between them (based on correlation of source-water density with overturning strength). Only when the region of deep convection moves significantly further south does AABW strength become larger than PI (60–70 kyr and 20–30 kyr BP), even though density of AABW source waters varies with a precessional frequency. At these times both maximum NADW and AABW values are stronger than present. At other times during the glacial, ocean heat loss in the GIN Seas dominates NADW, which increases as temperatures cool.

Previous compilations of multi-proxy data from ocean sediment cores and corals suggest large variability in ocean large-scale circulation during the last glacial cycle (Rahmstorf, 2002). Three different ocean circulation types have been proposed based on such work: an interstadial ('warm') mode, a stadial ('cold') mode and a Heinrich ('off') mode (Sarnthein et al., 1994). In the interstadial mode NADW forms in the GIN Seas, whereas in the stadial mode NADW forms in the open North Atlantic. We obtain a similar shift in deep water formation, when 20–30 kyr BP relates to a stadial circulation and much of our simulated 30–60 kyr BP is similar to the proposed interstadial circulation. However, the model does not capture a significant overall decrease in NADW of a 'cold' mode, except when freshwater hosing is introduced to simulate the Heinrich 'off' mode (Fig. 7c,d). This is a finding common to several different models (Weber et al., 2007). Part of this may be the lack of North Atlantic background freshwater routing in the main model experiments described here, which may have been larger than present and would have influenced the local salinity distribution and reduced NADW formation/depth in our simulations, as well as increasing the variability of the AMOC throughout the glacial cycle. Conversely, there is also substantial uncertainty in the interpretation of these proxy records, which makes it difficult to be conclusive about the general state of the AMOC during the last glacial cycle.

4. Conclusions

We present here the methodology and first results for HadCM3 climate simulations covering the last glacial cycle. By using a full resolution coupled ocean–atmosphere GCM we can obtain decent resolution at regional climate change scales, but with the drawback of not performing fully transient simulations. These simulations provide an estimation of climate changes on orbital timescales for the last glacial cycle that can be compared to ice-core records and other proxies of past climate change.

We obtain reasonable estimates of the global temperature G-IG range and trends in polar temperatures, although the magnitude of change at high latitudes is underestimated (as other similar models have found for the LGM). For example, Greenland LGM temperature anomalies in the model are only slightly more than half the estimated cooling from ice-core temperature reconstructions. However, for a more direct comparison with ice-core temperature reconstructions a precipitation weighting method was used to account for glacial–interglacial changes in seasonal accumulation. Using this method it was found that the greater the temperature decrease, the more the precipitation weighting negated the actual temperature decrease due to changes in precipitation seasonality. Polar amplification of global temperature change alters substantially with the inclusion of ice sheets, becoming asymmetric at North and South Poles. Antarctic polar amplification is more constant through time with varying ice sheets, at just under twice the global change.

One of the main caveats to our simulations is the lack of freshwater input into the North Atlantic to represent millennial-scale temperature changes. Feedbacks from changes in ocean circulation in our base-state simulations constitute 2–3 °C cooling over Greenland and the polar North Atlantic. The inclusion of freshwater background routing further cool these regions and significantly reduce the discrepancy between model and data. Other limitations are the lack of vegetation and atmospheric aerosol/dust feedbacks, as well as the unavoidable use of pre-industrial initial conditions. The use of the same initial conditions for all simulations, while not ideal, at least provides a consistent starting point, and enables the simulations to be run simultaneously (otherwise this sort of study would not be possible with a GCM).

The experiments presented here provide a novel dataset with which to analyse the mechanisms of orbital-scale climate change over the last glacial cycle. They do not represent a best estimate of a glacial–interglacial climate change reconstruction, as several key feedback processes are missing. In addition it is important to note that only one climate model has been used. As mentioned in previous sections, models have displayed different sensitivities to glacial boundary conditions in terms of NADW (Weber et al., 2007), and polar amplification (Masson-Delmotte et al., 2006b), for example. However, the simulations presented here can be used to investigate the sensitivity and climate interactions of HadCM3 to

different orbital and ice-sheet boundary conditions. So far we have performed an evaluation of the model temperature trends, and examined large-scale features in the climate system, namely polar amplification and ocean overturning circulation. However, there is a large amount of information within these large model datasets which can be used to investigate interactions and feedbacks in more detail. These will be presented in future publications. We also intend in future and current projects to examine the sensitivity of the climate system to the different ice-sheet reconstructions covering the last glacial cycle. Otto-Bliesner et al. (2006b) previously demonstrated that differences in ice-sheet height over Canada between ICE-5G and the previous ICE-4G reconstructions can have significant impacts on Pacific temperatures and wind structure for the LGM. Similarly, ice-sheet extent has been found to be important (Abe-Ouchi et al., 2007). Neither extent nor topography of ice sheets is well constrained prior to the LGM. We additionally will investigate the response to freshwater input (Heinrich iceberg discharge) under different initial base states (Singarayer et al., in preparation), and we are currently in the process of modelling vegetation distribution, carbon storage and methane emissions given the G-IG climate changes described in this paper.

Acknowledgements

The authors would like to thank Renato Spahni for trace gas data and Richard Peltier for ice-sheet reconstructions (the LGM to modern reconstructions are available at http://www.atmosp.physics.utoronto.ca/~peltier/data.php, and an example of the longer time sequence is available at: http://www.sbl.statkart.no/projects/pgs/ice_models/Peltier_ICE-5G_v1.2/), Valerie Masson-Delmotte for the GRIP temperature reconstruction, and the British Broadcasting Corporation (BBC) for commissioning the simulations for their TV series, *The Incredible Human Journey*.

References

Abe-Ouchi, A., Segawa, T., Saito, F., 2007. Climatic conditions for modelling the Northern Hemisphere ice sheets throughout the ice age cycle. Clim. Past 3, 423–438.

ACIA, 2004. Impacts of a Warming Arctic: Arctic Climate Impact Assessment. Cambridge University Press.

Berger, A., Loutre, M.F., 1991. Insolation values for the climate of the last 10 million years. Quat. Sci. Rev. 10, 297–317.

Berger, A., Loutre, M.F., Gallee, H., 1998. Sensitivity of the LLN climate model to the astronomical and CO_2 forcings over the last 200 ky. Clim. Dyn 14, 615–629.

Bigg, G.R., Wadley, M.R., Stevens, D.P., Johnson, J.A., 1998. Simulations of two last glacial maximum ocean states. Paleoceanography 13, 340–351.

Braconnot, P., Otto-Bliesner, B., Harrison, S., Joussaume, S., Peterchmitt, J.-Y., Abe-Ouchi, A., Crucifix, M., Driesschaert, E., Fichefet, Th., Hewitt, C.D., Kageyama, M., Kitoh, A., Laîné, A., Loutre, M.-F., Marti, O., Merkel, U., Ramstein, G., Valdes, P., Weber, S.L., Yu, Y., Zhao, Y., 2007a. Results of PMIP2 coupled simulations of the Mid-Holocene and Last Glacial Maximum – Part 1: experiments and large-scale features. Clim. Past 3, 261–277.

Braconnot, P., Otto-Bliesner, B., Harrison, S., Joussaume, S., Peterchmitt, J.-Y., Abe-Ouchi, A., Crucifix, M., Driesschaert, E., Fichefet, Th., Hewitt, C.D., Kageyama, M., Kitoh, A., Loutre, M.-F., Marti, O., Merkel, U., Ramstein, G., Valdes, P., Weber, L., Yu, Y., Zhao, Y., 2007b. Results of PMIP2 coupled simulations of the Mid-Holocene and Last Glacial Maximum – Part 2: feedbacks with emphasis on the location of the ITCZ and mid- and high latitudes heat budget. Clim. Past 3, 279–296.

Cattle, H., Crossley, J., 1995. Modelling Arctic climate-change. Philos. Trans. Royal Soc. A 352, 201–213.

Cox, P.M., Betts, R.A., Bunton, C.B., Essery, R.L.H., Rowntree, P.R., Smith, J., 1999. The impact of new land surface physics on the GCM simulation of climate and climate sensitivity. Clim. Dyn 15, 183–203.

Crucifix, M., Hewitt, C.D., 2005. Impact of vegetation changes on the dynamics of the atmosphere at the Last Glacial Maximum. Clim. Dyn 25, 447–459.

Curry, W.B., Oppo, D.W., 2005. Glacial water mass geometry and the distribution of delta C-13 of Sigma CO_2 in the western Atlantic Ocean. Paleoceanography 20, PA1017.

Dahl-Jensen, D., Mosegaard, K., Gundestrup, N., Clow, G.D., Johnsen, S.J., Hansen, A.W., Balling, N., 1998. Past temperatures directly from the Greenland ice sheet. Science 282, 268–271.

Edwards, J.M., Slingo, A., 1996. Studies with a flexible new radiation code.1. Choosing a configuration for a large-scale model. Q.J. Royal Met. Soc 122, 689–719.

EPICA community members, 2004. Eight glacial cycles from an Antarctic ice core. Nature 429, 623–862.

Gallee, H., Vanypersele, J.P., Fichefet, T., Marsiat, I., Tricot, C., Berger, A., 1992. Simulation of the last glacial cycle by a coupled, sectorially averaged climate–ice sheet model. 2. Response to insolation and CO_2 variations. J. Geophys. Res. 97, 15713–15740.

Gent, P.R., McWilliams, J.C., 1990. Isopycnal mixing in ocean circulation models. J. Phys. Oceanogr 20, 150–155.

Genthon, C., Barnola, J.M., Raynaud, D., Lorius, C., Jouzel, J., Barkov, N.I., Korotkevich, Y.S., Kotlyakov, V.M., 1987. Vostok ice core: climatic response to CO_2 and orbital forcing changes over the last climatic cycle. Nature 329, 414–418.

Gersonde, R., Crostab, X., Abelmann, A., Armand, L., 2005. Sea-surface temperature and sea ice distribution of the Southern Ocean at the EPILOG Last Glacial Maximum — a circum-Antarctic view based on siliceous microfossil records. Quat. Sci. Rev. 25, 869–896.

Gordon, C., Cooper, C., Senior, C.A., Banks, H., Gregory, J.M., Johns, T.C., Mitchell, J.F.B., Wood, R.A., 2000. The simulation of SST, sea ice extents and ocean heat transports in a version of the Hadley Centre coupled model without flux adjustments. Clim. Dyn 16, 147–168.

Hargreaves, J.C., Abe-Ouchi, A., Annan, J.D., 2007. Linking glacial and future climates through an ensemble of GCM simulations. Clim. Past 3, 77–87.

Hemming, S.R., 2004. Heinrich events: massive late Pleistocene detritus layers of the North Atlantic and their global climate imprint. Rev. Geophys 42 (1), RG1005.

Hewitt, C.D., Broccoli, A.J., Mitchell, J.F.B., Stouffer, R.J., 2001. A coupled model study of the last glacial maximum: was part of the North Atlantic relatively warm? Geophys. Res. Lett. 28, 1571–1574.

Hewitt, C.D., Broccoli, A.J., Crucifix, M., Gregory, J.M., Mitchell, J.F.B., Stouffer, R.J., 2006. The effect of a large freshwater perturbation on the glacial North Atlantic Ocean using a coupled general circulation model. J. Clim 19, 4436–4447.

Holden P.B., Edwards N.R., Wolff E.W., Valdes P.J., Singarayer J.S., submitted. West Antarctic Ice Sheet retreat could explain southern warmth in recent interglacials. Nature Geosciences (submitted).

Holland, M.M., Bitz, C.M., 2003. Polar amplification of climate change in coupled models. Clim. Dyn 21, 221–232.

IPCC: Climate Change, 2001. Impacts, Adaptation and Vulnerability – Contribution of Working Group II to the Third Assessment Report of IPCC. Cambridge University Press.

IPCC: Climate Change, 2007. The Physical Science Basis – Contribution of Working Group I to the Fourth Assessment Report of the IPCC. Cambridge University Press.

Jackson, C.S., Broccoli, A.J., 2003. Orbital forcing of Arctic climate: mechanisms of climate response and implications for continental glaciation. Clim. Dyn 21, 539–557.

Jansen, E., Overpeck, J., Briffa, K.R., Duplessy, J.-C., Joos, F., Masson-Delmotte, V., Olago, D.O., Otto-Bliesner, B., Peltier, W.R., Rahmstorf, S., Ramesh, R., Raynaud, D., Rind, D.H., Solomina, O., Villalba, R., Zhang, D., 2007. Palaeoclimate. In: Solomon, S., Qin, D., Manning, M., Chen, Z., Marquis, M., Averyt, K.B., Tignor, M., Miller, H.L. (Eds.), Climate Change 2007: The Physical Science Basis. Contribution of Working Group I to the Fourth Assessment Report of the Intergovernmental panel on Climate Change. Cambridge University Press, Cambridge, UK, and New York, pp. 433–497.

Jouzel, J., Masson-Delmotte, V., Cattani, O., Dreyfus, G., Falourd, S., Hoffmann, G., Minster, B., Nouet, J., Barnola, J.M., Chappellaz, J., Fischer, H., Gallet, J.C., Johnsen, S., Leuenberger, M., Loulergue, L., Luethi, D., Oerter, H., Parrenin, F., Raisbeck, G., Raynaud, D., Schilt, A., Schwander, J., Selmo, E., Souchez, R., Spahni, R., Stauffer, B., Steffensen, J.P., Stenni, B., Stocker, T.F., Tison, J.L., Werner, M., Wolff, E.W., 2007. Orbital and millennial Antarctic climate variability over the past 800,000 years. Science 317, 793–796.

Kawamura, K., Parrenin, F., Lisiecki, L., Uemura, R., Vimeux, F., Severinghaus, J.P., Hutterli, M.A., Nakazawa, T., Aoki, S., Jouzel, J., Raymo, M.E., Matsumoto, K., Nakata, H., Motoyama, H., Fujita, S., Goto-Azuma, K., Fujii, Y., Watanabe, O., 2007. Northern Hemisphere forcing of climatic cycles in Antarctica over the past 360,000 years. Nature 448, 912–916.

Krinner, G., Genthon, C., 1999. Altitude dependence of the ice sheet surface climate. Geophys. Res. Lett. 26, 2227–2230.

Krinner, G., Werner, M., 2003. Impact of precipitation seasonality changes on isotopic signals in polar ice cores. Earth Planet Sci. Lett. 216, 525–538.

Kutzbach, J.E., Liu, X.D., Liu, Z.Y., Chen, G.S., 2008. Simulation of the evolutionary response of global summer monsoons to orbital forcing over the past 280,000 years. Clim. Dyn 30, 567–579.

Lorenz, S.J., Lohmann, G., 2004. Acceleration technique for Milankovitch type forcing in a coupled atmosphere–ocean circulation model: method and application for the Holocene. Clim. Dyn 23, 727–743.

Liu, Z., Otto-Bliesner, B., He, F., Brady, E.C., Tomas, R., Clark, P.U., Carlson, A.E., Lynch-Stieglitz, J., Curry, W., Brook, E., Erickson, D., Jacob, R., Kutzbach, J., Cheng, J., 2009. Transient simulation of last deglaciation with a new mechanism for Bolling–Allerod warming. Science 325, 310–314.

Loulergue, L., Schilt, A., Spahni, R., Masson-Delmotte, V., Blunier, T., Lemieux, B., Barnola, J.-M., Raynaud, D., Stocker, T.F., Chappellaz, J., 2008. Orbital and

millennial-scale features of atmospheric CH4 over the past 800,000 years. Nature 453, 383–386.
Lunt, D.J., Williamson, M.S., Valdes, P.J., Lenton, T., Marsh, R., 2006. Comparing transient, accelerated, and equilibrium simulations of the last 30 000 years with the GENIE-1 model. Clim. Past 2, 221–235.
Masson, V., Vimeux, F., Jouzel, J., Morgan, V., Delmotte, M., Ciais, P., Hammer, C., Johnsen, S., Lipenkov, V.Y., Mosley-Thompson, E., Petit, J.R., Steig, E.J., Stievenard, M., Vaikmae, R., 2000. Holocene climate variability in Antarctica based on 11 ice-core isotopic records. Quat. Res. 54, 348–358.
Masson-Delmotte, V., Jouzel, J., Landais, A., Stievenard, M., Johnsen, S.J., White, J.W.C., Sveinbjornsdottir, A., Fuhrer, K., 2005. Deuterium excess reveals millennial and orbital scale fluctuations of Greenland moisture origin. Science 309, 118–121.
Masson-Delmotte, V., Dreyfus, G., Braconnot, P., Johnsen, S., Jouzel, J., Kageyama, M., Landais, A., Loutre, M.F., Nouet, J., Parrenin, F., Raynaud, D., Stenni, B., Tuenter, E., 2006a. Past temperature reconstructions from deep ice cores: relevance for future climate change. Clim. Past 2, 145–165.
Masson-Delmotte, V., Kageyama, M., Braconnot, P., Charbit, S., Krinner, G., Ritz, C., Guilyardi, E., Jouzel, J., Abe-Ouchi, A., Crucifix, M., Gladstone, R.M., Hewitt, C.D., Kitoh, A., LeGrande, A.N., Marti, O., Merkel, U., Motoi, T., Ohgaito, R., Otto-Bliesner, B., Peltier, W.R., Ross, I., Valdes, P.J., Vettoretti, G., Weber, S.L., Wolk, F., Yu, Y., 2006b. Past and future polar amplification of climate change: climate model intercomparisons and ice-core constraints. Clim. Dyn 26, 513–529.
Martinerie, P., Lipenkov, V.Y., Raynaud, D., 1994. Air content paleo record in the Vostok ice core (Antarctica): a mixed record of climatic and glaciological parameters. J. Geophys. Res. 99, 10565–10576.
Martinsen, D.G., Pisias, N.G., Hays, J.D., Imbrie, J., Moore Jr., T.C., Shackleton, N.J., 1987. Age dating and orbital theory of the ice ages: development of a high resolution 0–300,000-year chronostratigraphy. Quat. Res. 27, 1–30.
McManus, J.F., Oppo, D.W., Keigwin, L.D., Cullen, J.L., Bond, G.C., 2002. Thermohaline circulation and prolonged interglacial warmth in the North Atlantic. Quat. Res. 58, 17–21.
McManus, J.F., Francois, R., Gherardi, J.M., Keigwin, L.D., Brown-Leger, S., 2004. Collapse and rapid resumption of Atlantic meridional circulation linked to deglacial climate changes. Nature 428, 834–837.
Meissner, K.J., Clark, P.U., 2006. Impact of floods versus routing events on the thermohaline circulation. Geophys. Res. Lett 33, L15704.
Otto-Bliesner, B.L., Marsha, S.J., Overpeck, J.T., Miller, G.H., Hu, A.X., 2006a. Simulating arctic climate warmth and icefield retreat in the last interglaciation. Science 311, 1751–1753.
Otto-Bliesner, B.L., Brady, E.C., Clauzet, G., Tomas, R., Levis, S., Kothavala, Z., 2006b. Last Glacial Maximum and Holocene climate in CCSM3. J. Clim 19, 2526–2544.
Otto-Bliesner, B.L., Hewitt, C.D., Marchitto, T.M., Brady, E., Abe-Ouchi, A., Crucifix, M., Murakami, S., Weber, S.L., 2007. Last Glacial Maximum ocean thermohaline circulation: PMIP2 model intercomparisons and data constraints. Geophys. Res. Lett 34, L12706. doi:10.1029/2007GL029475.
Overpeck, J.T., Otto-Bliesner, B.L., Miller, G.H., Muhs, D.R., Alley, R.B., Kiehl, J.T., 2006. Paleoclimatic evidence for future ice-sheet instability and rapid sea-level rise. Science 311, 1747–1750.
Parrenin, F., Barnola, J.-M., Beer, J., Blunier, T., Castellano, E., Chappellaz, J., Dreyfus, G., Fischer, H., Fujita, S., Jouzel, J., Kawamura, K., Lemieux-Dudon, B., Loulergue, L., Masson-Delmotte, V., Narcisi, B., Petit, J.-R., Raisbeck, G., Raynaud, D., Ruth, U., Schwander, J., Severi, M., Spahni, R., Steffensen, J.P., Svensson, A., Udisti, R., Waelbroeck, C., Wolff, E., 2007. The EDC3 agescale for the EPICA dome C ice core. Clim. Past 3, 485–497.
Peltier, W.R., 2004. Global glacial isostasy and the surface of the iceage Earth: the ICE-5G (VM2) model and GRACE. Annu. Rev. Earth Planet Sci. 32, 111–149.
Peltier, W.R., Fairbanks, R.G., 2006. Global glacial ice volume and Last Glacial Maximum duration from an extended Barbados sea level record. Quat. Sci. Rev. 25, 3322–3337.
Petit, J.R., Jouzel, J., Raynaud, D., Barkov, N.I., Barnola, J.-M., Basile, I., Bender, M., Chappellaz, J., Davis, J., Delaygue, G., Delmotte, M., Kotlyakov, V.M., Legrand, M., Lipenkov, V., Lorius, C., Pepin, L., Ritz, C., Saltzman, E., Stievenard, M., 1999. Climate and atmospheric history of the past 420 000 years from the Vostok Ice Core, Antarctica. Nature 399, 429–436.
Pope, V.D., Gallani, M.L., Rowntree, P.R., Stratton, R.A., 2000. The impact of new physical parameterisations in the Hadley Centre climate model: HadAM3. Clim. Dyn 16, 123–146.
Rahmstorf, S., 2002. Ocean circulation and climate during the past 120,000 years. Nature 419, 207–214.
Rahmstorf, S., Crucifix, M., Ganopolski, A., Goosse, H., Kamenkovich, I., Knutti, R., Lohmann, G., Marsh, R., Mysak, L.A., Wang, Z.M., Weaver, A.J., 2005. Thermohaline circulation hysteresis: a model intercomparison. Geophys. Res. Lett 32, L23605.
Sarnthein, M., Winn, K., Jung, s.J.A., Duplessy, J.C., Labeyrie, L., Erlenkeuser, H., Genssen, G., 1994. Changes in East Atlantic deep-water circulation over the last 30,000 years – 8 time slice reconstructions. Paleoceanography 9, 209–267.
Sarnthein, M., Pflaumann, U., Weinelt, M., 2003. Past extent of sea ice in the northern North Atlantic inferred from foraminiferal paleotemperature estimates. Paleoceanography 18 (2), 1047.
Short, D.A., Mengel, J.G., 1986. Tropical climatic phase lags and earths precession cycle. Nature 323, 48–50.
Singarayer et al., in preparation. Relative impacts of orbital- and millennial-scale climate change on late Quaternary humid-arid phases in Southern Africa. Quat. Sci. Rev. (in preparation).
Spahni, R., Chappellaz, J., Stocker, T.F., Loulergue, L., Hausammann, G., Kawamura, K., Fluckiger, J., Schwander, J., Raynaud, D., Masson-Delmotte, V., Jouzel, J., 2005. Variations of atmospheric methane and nitrous oxide during the last 650 000 years from Antarctic ice cores. Science 310, 1317–1321.
Stouffer, R.J., Manabe, S., 2003. Equilibrium response of thermohaline circulation to large changes in atmospheric CO_2 concentration. Clim. Dyn 20, 759–773.
Tarasov, L., Peltier, W.R., 1999. Impact of thermomechanical ice sheet coupling on a model of the 100 kyr ice age cycle. J. Geophys. Res. Atmos 104, 9517–9545.
Tarasov, L., Peltier, W.R., 2002. Greenland glacial history and local geodynamic consequences. Geophys. J. Int 150, 198–229.
Trenberth, K.E., Jones, P.D., Ambenje, P., Bojariu, R., Easterling, D., Klein Tank, A., Parker, D., Rahimzadeh, F., Renwick, J.A., Rusticucci, M., Soden, B., Zhai, P., 2007. Observations: surface and atmospheric climate change. In: Solomon, S., Qin, D., Manning, M., Chen, Z., Marquis, M., Averyt, K.B., Tignor, M., Miller, H.L. (Eds.), Climate Change 2007: The Physical Science Basis. Contribution of Working Group I to the Fourth Assessment Report of the Intergovernmental Panel on Climate Change. Cambridge University Press, Cambridge, UK, and New York.
Vellinga, M., Wood, R.A., 2002. Global climatic impacts of a collapse of the Atlantic thermohaline circulation. Climatic Change 54, 251–267.
Weber, S., Drijfhout, S., Abe-Ouchi, A., Crucifix, M., Eby, M., Ganopolski, A., Murakami, S., Otto-Bliesner, B., Peltier, W.R., 2007. The modern and glacial overturning circulation in the Atlantic Ocean in PMIP coupled model simulations. Clim. Past 3, 51–64.